Spin order in the charge disproportionated phases of the *A*-site layer ordered triple perovskite $LaCa_2Fe_3O_9$

Angel M. Arevalo-Lopez,[1,*] Yoshiteru Hosaka,[2] Haichuan Guo,[2] Fabio Denis Romero,[2,3] Takashi Saito,[2] J. Paul Attfield,[4] and Yuichi Shimakawa[2,†]

[1]*Université Lille, CNRS, Centrale Lille, ENSCL, Université Artois, UMR 8181–UCCS–Unité de Catalyse et Chimie du Solide, F-59000 Lille, France*

[2]*Institute for Chemical Research, Kyoto University, Gokasho, Uji, Kyoto 611-0011, Japan*

[3]*Hakubi Center for Advanced Research, Kyoto University, Yoshida-honmachi, Sakyo-ku, Kyoto 606-8501, Japan*

[4]*Centre for Science at Extreme Conditions and School of Chemistry, University of Edinburgh, Peter Guthrie Tait Road, The King's Buildings, EH9 3FD, Edinburgh, United Kingdom*

(Received 11 September 2017; revised manuscript received 24 November 2017; published 19 January 2018)

The coupling between spins and charge disproportionation states has been investigated in the $LaCa_2Fe_3O_9$ oxide with neutron powder diffraction. This *A*-site layer ordered triple perovskite $LaCa_2Fe_3O_9$ undergoes charge disproportionation on cooling and shows two different charge ordering patterns. At 230 K, $Fe^{3.67+}$ disproportionates into a 2:1 ratio of Fe^{3+} : Fe^{5+}, which order in a layered manner along the ⟨010⟩ direction of the pseudocubic unit cell. At lower temperatures ($T < 170$ K), the charge ordering pattern changes to a layered arrangement along the ⟨111⟩ direction. Neutron powder diffraction data show that in the intermediate temperature range (170 K $< T <$ 230 K) the spins order into a cycloidal structure on the *ac* plane for the Fe^{3+} cations while the Fe^{5+} cations remain paramagnetic. For the lowest temperature range (2 K $< T <$ 190 K), the spin structure follows the charge ordering and evolves to a ⟨111⟩ layered magnetic structure.

DOI: 10.1103/PhysRevB.97.024421

I. INTRODUCTION

Charge ordering is often observed in transition-metal oxide systems with electronic instabilities of mixed-valence cations. The Verwey transition of Fe_3O_4 with Fe^{2+}/Fe^{3+} order is a famous example and the phenomenon is evidenced by a drastic change in transport properties [1–3]. Similar charge ordering behaviors are observed in a few oxides containing unusually high-valence cations due to charge disproportionation (CD) of Fe^{4+}. The perovskite $CaFeO_3$ shows a metal-insulator transition at 290 K due to CD of Fe^{4+} to Fe^{3+} and Fe^{5+} which order in a rocksalt-type arrangement. The CD transition in $CaFeO_3$ changes the uniform $Fe^{4+}O_6$ octahedra to alternating large $Fe^{3+}O_6$ and small $Fe^{5+}O_6$ octahedra; thus the charge order is coupled with the lattice degree of freedom [4,5]. Other examples of CD in Fe-containing perovskite-structure oxides include rocksalt ordered Fe^{3+}/Fe^{5+} in the *A*-site ordered $CaCu_3Fe_4O_{12}$ and checkerboard ordered Fe^{3+}/Fe^{5+} in the *B*-site layer ordered Ca_2FeMnO_6 [6,7]. The CD in high-valence Fe has been rationalized as the localization of ligand holes which are produced by strong hybridization of Fe *d* with O *p* orbitals [8,9].

An important aspect of CD behavior concerns coupling of the charge and spin degrees of freedom. In $CaFeO_3$ a magnetic transition occurs at 210 K, below the CD transition temperature, and a helical magnetic structure of Fe^{3+}/Fe^{5+} spins is stabilized [5]. In the *A*-site ordered quadruple perovskite $CaCu_3Fe_4O_{12}$, on the other hand, the magnetic transition temperature is the same as the CD transition temperature, and the Fe^{3+} and Fe^{5+} spins couple ferromagnetically below the CD transition temperature giving rise to ferrimagnetism when coupled with the Cu ions [10,11]. In the *B*-site layered double perovskite Ca_2FeMnO_6, three-dimensional noncollinear magnetic order develops below 95 K, although the two-dimensional CD of Fe^{4+} occurs at 200 K [7]. As can be observed, the coupling between the charge and spins in the CD transition varies significantly between oxides containing high-valence Fe ions.

Very recently we found that an *A*-site layered triple perovskite $LaCa_2Fe_3O_9$ shows CD from high-valence $Fe^{3.67+}$ to a 2:1 ratio of Fe^{3+} and Fe^{5+} [12]. Interestingly, the compound shows two successive structural transitions due to different CD ordering patterns. The first transition occurs at 230 K, where the charge disproportionated 2:1 Fe^{3+} and Fe^{5+} are ordered in a layered manner, along the ⟨010⟩ layer stacking direction of the pseudocubic unit cell. Below the second transition at 170 K, the charge disproportionated 2:1 Fe^{3+} and Fe^{5+} are ordered along the ⟨111⟩ direction of the pseudocubic unit cell. Magnetic susceptibility data collected as a function of temperature show that both transitions occur at the same temperatures as the magnetic anomalies [12]. The simple perovskite $La_{1/3}Ca_{2/3}FeO_3$ with identical chemical composition to that of the present $LaCa_2Fe_3O_9$, but with random arrangement of the *A*-site La and Ca ions, presents only one structural transition at 217 K to a 2:1 Fe^{3+} and Fe^{5+} charge ordering pattern along the ⟨111⟩ direction of the pseudocubic perovskite unit cell, similar to the one found at the lowest temperatures in the *A*-site layer ordered analog [13]. The magnetic structures of the CD states have not been determined.

*angel.arevalo-lopez@univ-lille1.fr
†shimak@scl.kyoto-u.ac.jp

In this study, we analyzed the magnetic structures of this layered compound which shows unusual CD behaviors. Using neutron powder diffraction data, we have revealed that the two charge ordering patterns result in different magnetic structures. The magnetic structures of $LaCa_2Fe_3O_9$ and $La_{1/3}Ca_{2/3}FeO_3$ are compared to observe the effects of the cation ordering upon the spin orders.

II. EXPERIMENT

The synthesis of $LaCa_2Fe_3O_9$ and $La_{1/3}Ca_{2/3}FeO_3$ was carried out as reported previously [12,13]. Powder neutron diffraction patterns from both samples were measured using the time-of-flight neutron diffractometer WISH at the ISIS spallation source [14]. Data were collected every 50 K between 2 and 300 K and every 5 K in the 150 K $< T <$ 250 K temperature range on warming. All the data were normalized using the MANTIDPLOT program [15]. Crystal and magnetic structures were refined using the FULLPROF suite software package [16]. Symmetry analysis was performed with BASIRREPS within the same software.

III. RESULTS AND DISCUSSION

Figure 1(a) shows the neutron diffraction patterns (bank 2) as a function of temperature from 250 to 150 K collected using the WISH diffractometer on warming. The evolution of two different phases due to the successive transitions at 230 and 170 K reported in our previous study can clearly be seen and the patterns are colored in red and blue, respectively [12].

Neutron diffraction data collected at 300 K were fitted well using the structure reported previously [12]. It consists of an $a' = a + b$, $b' = 6c$, $c' = -a + b$*Pnma* supercell model (with $|a| = |b| = |c| = a_p$ being the lattice parameter of the simple perovskite structure ≈3.8 Å), necessary to account for the 2:1 layered *A*-site ordering between Ca and La and the octahedral tilting. The refined occupancies for the La and Ca are 0.67(1)/0.33 and 0.18(1)/0.82 for the different *A* sites, in agreement with our synchrotron x-ray diffraction (SXRD) results, thus confirming the *A*-site layered structure. The structure is reported in Table 1 in the Supplemental Material [17]. The absence of vacancies at any of the oxygen sites is also confirmed by the neutron refinement.

The structural model accounts for all the observed reflections in data collected from $LaCa_2Fe_3O_9$ at temperatures in the range 240 K $\leqslant T \leqslant$ 300 K. Figure 2, top, shows the long *d*-spacing bank of the diffraction data at 240 K; other banks and *R* factors are shown in the Supplemental Material (Fig. S1) [17]. Although additional superstructure diffraction peaks appear below 230 K, the nuclear diffraction peaks originating from the *Pnma* supercell fit well the essential diffraction maxima and show a cell-volume decrease at 230 K and an increase at 190 K [Fig. 1(b)]. These temperature-dependent changes in the crystal structure are consistent with those observed in SXRD data in our previous study [12].

At least five additional diffraction maxima were clearly observed when the sample was cooled below 230 K as shown in Fig. 1(a). These features are not present in SXRD data collected from $LaCa_2Fe_3O_9$ in the temperature range 170 K $<$ $T <$ 230 K, suggesting the origin of these peaks is likely

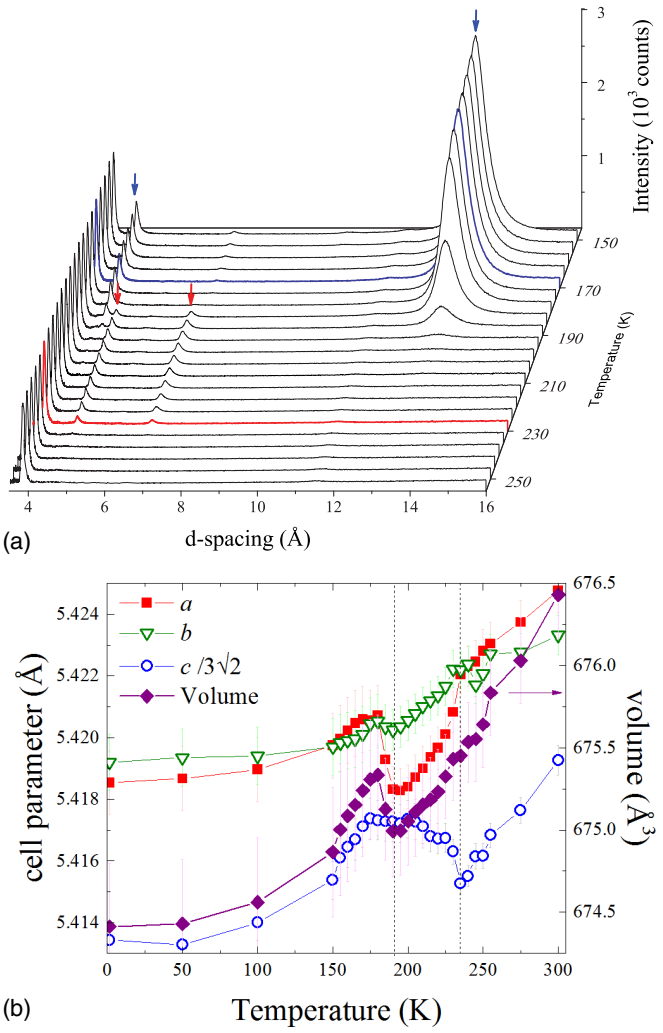

FIG. 1. (a) Thermal evolution of the NPD patterns between 150 and 250 K on warming. Magnetic Bragg reflections are marked with arrows; the colored patterns show the transition temperatures observed by magnetometry at 230 and 170 K (red and blue arrows, respectively). (b) Temperature dependence of the lattice parameters and the volume from NPD data of $LaCa_2Fe_3O_9$ with both CD/magnetic transitions marked by dashed lines. The transition temperatures appear at 190 and 235 K here. They differ from the previously reported 170 and 230 K values due to possible differences in warming rate or thermal equilibration in the previous experiments.

magnetic [12]. Mössbauer spectroscopy data collected in this temperature range show the presence of Fe^{3+} and Fe^{5+} in a 2:1 ratio and that the Fe^{3+} spins are magnetically ordered while the Fe^{5+} spins remain paramagnetic. Therefore, an additional magnetic model was included in the fit to the observed neutron powder diffraction (NPD) in the range 190 K $< T <$ 230 K.

All the additional magnetic reflections can be indexed with the propagation vector $k_1 = [1/3\ 1/3\ 1/3]$ on a cubic $a_p \times a_p \times a_p$ cell, or with $k_{1'} = [1/3\ 0\ 0]$ on the *Pnma* supercell that allows for the layered ordering of La^{3+} and Ca^{2+} cations. As mentioned earlier, our Mössbauer study shows that the Fe^{5+} spins are not long range ordered (idle) in this temperature range; thus the Fe^{3+} spins are ordered below the CD transition temperature, whereas the Fe^{5+} spins remain paramagnetic. We

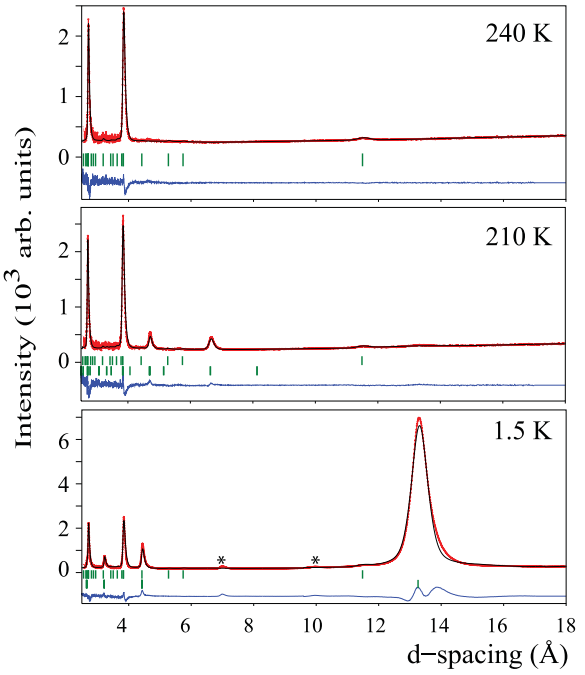

FIG. 2. $LaCa_2Fe_3O_9$ Rietveld refinement plots of neutron powder-diffraction data collected on WISH@ISIS at 240, 210, and 1.5 K. The observed (red dots), calculated (black lines), and difference (blue lines) patterns are shown. The allowed Bragg reflections (green vertical lines) for nuclear (top) and magnetic (bottom) phases are shown. Small asterisks mark magnetic diffraction from a secondary $CaFeO_3$ phase.

performed symmetry analysis [18]; irreducible representations are reported in Table 2 in the Supplemental Material [17]. The best refined magnetic structure ($R_{mag} = 2.9\%$ for bank 2) consists of a spin cycloid with 120° rotation along the (100) direction and a magnitude of 1.96(2) μ_B per Fe^{3+} as shown in Fig. 3(a). The Fe^{3+} magnetic layers are antiferromagnetically (AFM) coupled along the b axis and the spins are confined to the ac plane. Spin-density wave–like solutions are also plausible with R factors similar to the cycloid model and cannot be distinguished with powder data; however, there are no obvious reasons for the moments to take different values and Mössbauer results support only one magnetic moment value for the Fe^{3+}; therefore the spin cycloid was preferred. Fe^{5+} spins were constrained to zero values since refined moments were in the limit of detection (≈0.4 μ_B) and no significant improvement of the R factors was observed; this is also in accordance with Mössbauer data. After refinement of the magnetic structure, it was analyzed with FINDSYM [19]; the resulting magnetic space group is $Pmc2_1$. It is interesting that both the charge ordering pattern and the magnetic structure show two-dimensional features reflecting the A-site layered crystal structure.

Neutron powder diffraction data collected below $T_{N2} =$ 190 K, where the second structural transition due to the charge ordering pattern change from the ⟨010⟩ to ⟨111⟩ direction occurs, show additional reflections which increase in intensity down to the lowest temperature measured (1.5 K). These peaks were also assumed to be magnetic since our previous

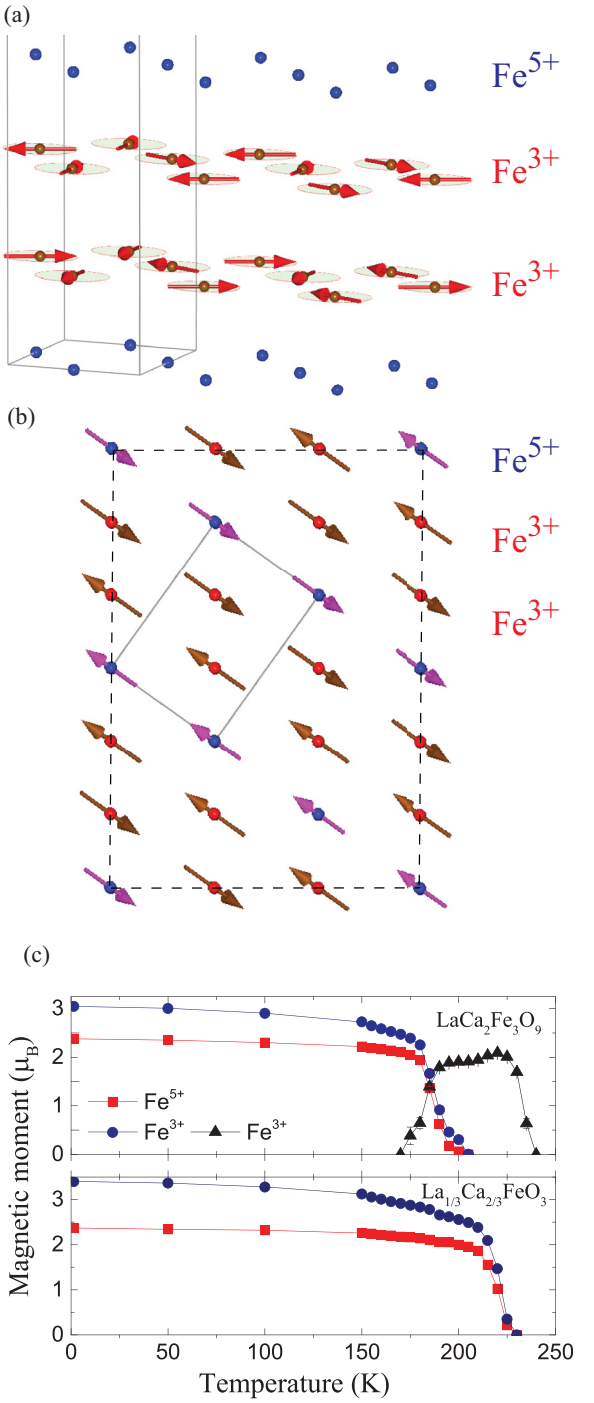

FIG. 3. (a) Magnetic structure of $LaCa_2Fe_3O_9$ in the intermediate phase, 170 K < T < 240 K. Fe^{5+} spins remain idle while Fe^{3+} spins order with a propagation vector $k_{1'} = (1/3, 0, 0)$ on a $Pnma$ cell (only half of the cell is shown). (b) Low-temperature magnetic structure of $LaCa_2Fe_3O_9$ (1.5 K < T < 200 K) and magnetic structure of $La_{1/3}Ca_{2/3}FeO_3$ ($T_N = 217$ K). Both Fe^{3+} and Fe^{5+} order on a triple layered antiferromagnetic structure with a propagation vector $k_{2'} = (0, 0, \frac{1}{2})$ on a $\sqrt{2}a_p \times \sqrt{2}a_p \times \sqrt{3}a_p$ hexagonal cell shown with lines. Dashed lines show the $3\sqrt{2}a_p \times 3\sqrt{2}a_p \times 6a_p$ supercell needed to account for the CD 2:1 Fe^{3+} : Fe^{5+}, layered A-site cation ordering and octahedral tilting. (c) Magnetic moment as function of temperature obtained from Rietveld refinement on $LaCa_2Fe_3O_9$ and the disordered $La_{1/3}Ca_{2/3}FeO_3$.

Mössbauer results indicated that both Fe^{3+} and Fe^{5+} spins are magnetically ordered at these temperatures and no additional reflections were observed in SXRD data. These reflections can be indexed with a propagation vector $k_2 = [1/6\ 1/6\ 1/6]$ on the $a_p \times a_p \times a_p$ cubic cell. To account for the charge ordering pattern, the refinement was performed with an equivalent description in an $a'' = a - b$, $b'' = b - c$, $c'' = a + b + c$, $\alpha = \beta = 90^\circ$, $\gamma = 120^\circ$ hexagonal cell with a propagation vector $k_{2'} = [0\ 0\ \frac{1}{2}]$. Symmetry analysis was performed (Supplemental Material, Table 4 [17]) and the best refined low-temperature magnetic-structure model is shown in Fig. 3(b) ($R_{mag} = 5.9\%$ for bank 2). The spins of the charge disproportionated Fe^{3+} and Fe^{5+} ions, which adopt a 2:1 layered arrangement along the $\langle 111 \rangle$ direction of the pseudocubic unit cell, are also ordered in a collinear way. The refined moments at 1.5 K are 3.0(1) and 2.4(1) μ_B for Fe^{3+} and Fe^{5+}, respectively. The spins of Fe^{3+} and Fe^{5+} within each layer are ferromagnetically (FM) ordered and this triple-layered spin structure is AFM stacked along the same $\langle 111 \rangle$ direction. Because the spin direction of every triple layer is opposite, no net magnetization is given with this magnetic structure, which is consistent with the observed magnetic susceptibility at low temperatures [12]. The magnetic space group resulted in $C2/m$ within a $-a'' - 2b''$, $-a''$, $2c''$ monoclinic cell. Temperature dependencies of the magnetic moments are shown in Fig. 3(c). An important point is that the Fe^{3+}/Fe^{5+} magnetic structure drastically changes when the CD pattern changes.

As we reported previously, the A-site disordered analog $La_{1/3}Ca_{2/3}FeO_3$ shows the same charge ordering pattern along the $\langle 111 \rangle$ direction below 217 K [13]. As shown in Fig. S2b in the Supplemental Material [17], neutron powder diffraction data collected at 1.5 K of this disordered analogue are similar to those observed from $LaCa_2Fe_3O_9$ and the data are well accounted for using an identical magnetic structure ($R_{mag} = 4.04\%$ for bank 2). The refined moments at 1.5 K are 3.4(1) and 2.4(1) μ_B for Fe^{3+} and Fe^{5+}, respectively. Therefore, the ground-state CD patterns and magnetic structures are the same for the A-site layer ordered $LaCa_2Fe_3O_9$ and the A-site disordered $La_{1/3}Ca_{2/3}FeO_3$. The results also imply that the ground-state magnetic structures are primarily determined by the arrangement of Fe^{3+} and Fe^{5+} ions and their magnetic interactions, and are less influenced by the A-site order/disorder.

The unusual magnetic structure observed at intermediate temperatures, where only Fe^{3+} spins are ordered while the Fe^{5+} spins remain paramagnetic, is only stabilized in the A-site layer ordered compound. Taking into account the charge ordering pattern at the intermediate temperatures, which implies a 2:1 order of Fe^{3+} : Fe^{5+} along the $\langle 010 \rangle$ direction, a simple analysis with Goodenough-Kanamori-Anderson rules (GKA) explains the unusual spin cycloid magnetic structure. Considering the layered charge ordering pattern, the strongest interaction along the b axis is AFM between Fe^{3+} and Fe^{3+} (half-filled e_g orbitals) and frustrates the FM coupling to the Fe^{5+} (empty e_g orbitals) due to the magnetic periodicity along this direction. A similar magnetic frustration has been recently observed in the $Ca_{0.5}Bi_{0.5}Fe^{3.5+}O_3$ compound. This material shows CD of $Fe^{3.5+}$ to a 2:1 ratio of Fe^{3+}:$Fe^{4.5+}$ and the magnetic order shows AFM coupling between Fe^{3+} spins and idle $Fe^{4.5+}$ spins [20].

In conclusion, we have determined the intermediate and ground magnetic states in $LaCa_2Fe_3O_9$ which are both coupled to their respective CD patterns. The intermediate magnetic state shows an unusual spin cycloid with AFM layers of 120° rotating spins of Fe^{3+} and idle Fe^{5+} spins. The ground state, on the contrary, shows triple FM layers stacked AFM along the $\langle 111 \rangle$ direction. These magnetic structures are explained with the magnetic interactions according to the GKA rule. The disordered $La_{1/3}Ca_{2/3}Fe_3O_9$ presents the same magnetic ground state. The A-site order is responsible for the intermediate phase since this is not observed in the disordered analog; however, the ground state is very robust as the same magnetic structure is observed in both ordered and disordered compounds.

ACKNOWLEDGMENTS

This work was partly supported by Grants-in-Aid for Scientific Research (Grants No. 16H00888 and No. 16H02266) and by a grant for the Integrated Research Consortium on Chemical Sciences from the Ministry of Education, Culture, Sports, Science and Technology (MEXT) of Japan. The work was also supported by Japan Society for the Promotion of Science (JSPS) Core-to-Core Program (A) Advanced Research Networks and Japan Science and Technology Agency (JST), CREST, and by grants from the EPSRC. Support was also provided by the Royal Society and ICR's Short Term Exchange program. We also thank STFC for the provision of ISIS beam time, and Dr. Dmitry Khalyavin and Dr. Pascal Manuel for assistance with data collection.

[1] E. J. W. Verwey, Nature **144**, 327 (1939).
[2] E. J. W. Verwey and P. W. Haayman, Physica (Amsterdam) **8**, 979 (1941).
[3] M. S. Senn, J. P. Wright, and J. P. Attfield, Nature **481**, 173 (2012).
[4] M. Takano, N. Nkanishi, Y. Takeda, S. Naka, and T. Takada, Mater. Res. Bull. **12**, 923 (1977).
[5] P. M. Woodward, D. E. Cox, E. Moshopoulou, A. W. Sleight, and S. Morimoto, Phys. Rev. B. **62**, 844 (2000).
[6] I. Yamada, K. Takata, N. Hayashi, S. Shinohara, M. Azuma, S. Mori, S. Muranaka, Y. Shimakawa, and M. Takano, Angew. Chem., Int. Ed. **47**, 7032 (2008).
[7] Y. Hosaka, N. Ichikawa, T. Saito, P. Manuel, D. Khalyavin, J. P. Attfield, and Y. Shimakawa, J. Am. Chem. Soc. **137**, 7468 (2015).
[8] W.-T. Chen, T. Saito, N. Hayashi, M. Takano, and Y. Shimakawa, Sci. Rep. **2**, 449 (2012).
[9] Y. Shimakawa, J. Phys. D: Appl. Phys. **48**, 504006 (2015).
[10] M. Mizumaki, W. T. Chen, T. Saito, I. Yamada, J. P. Attfield, and Y. Shimakawa, Phys. Rev. B **84**, 094418 (2011).
[11] Y. Shimakawa and M. Mizumaki, J. Phys.: Condens. Matter **26**, 473203 (2014).
[12] H. Guo, Y. Hosaka, F. D. Romero, T. Saito, N. Ichikawa, and Y. Shimakawa, Inorg. Chem. **56**, 3695 (2017).

[13] H. Guo, Y. Hosaka, H. Seiki, T. Saito, N. Ichikawa, and Y. Shimakawa, J. Solid State Chem. **246**, 199 (2017).

[14] L. C. Chapon, P. Manuel, P. G. Radaelli, C. Benson, L. Perrot, S. Ansell, N. J. Rhodes, D. Raspino, D. Duxbury, E. Spill, and J. Norris, Neutron News **22**, 22 (2011).

[15] O. Arnold, J. C. Bilheux, J. M. Borreguero, A. Buts, S. I. Campbell, L. Chapon, M. Doucel, N. Draper, R. Ferraz Leal, M. A. Gigg, V. E. Lynch, A. Markvarsden, D. J. Mikkelson, R. Miller, K. Palmen, P. Parker, G. Passos, T. G. Perring, P. F. Peterson, S. Ren *et al.*, Nucl. Instrum. Methods Phys. Res., Sect. A **764**, 156 (2011).

[16] J. Rodriguez-Carvajal, Phys. B (Amsterdam, Neth.) **192**, 55 (1993).

[17] See Supplemental Material at http://link.aps.org/supplemental/10.1103/PhysRevB.97.024421 for other diffraction banks and temperature evolution of cell parameters for $LaCa_2Fe_3O_9$ and $La_{1/3}Ca_{2/3}FeO_3$. Structure and symmetry analysis are also presented in the tables.

[18] E. F. Bertaut, Acta Crystallogr. A **24**, 217 (1968).

[19] H. T. Stokes and D. M. Hatch, J. Appl. Crystallogr. **38**, 237 (2005).

[20] F. Denis Romero, Y. Hosaka, N. Ichikawa, T. Saito, G. McNally, J. P. Attfield, and Y. Shimakawa, Phys. Rev. B **96**, 064434 (2017).